East European Journal of Physics. 3. 454-465 (2025)
DOI:10.26565/2312-4334-2025-3-50 ISSN 2312-4334

INFLUENCE OF AN ADDITIONAL P3HT LAYER ON THE PERFORMANCE OF P3HT: $IC_{60}BA$ POLYMER SOLAR CELL

Chittur Devarajan Ramabadran[a,b§], K. Sebastian Sudheer[a]*
[a]*Department of Physics, Opto-electronic Device Simulation Research Lab, Christ College [Autonomous], Irinjalakuda, Thrissur, 680125, University of Calicut, Kerala, India*
[b]*Department of Physics, Government College, Chittur, Palakkad, 678104, University of Calicut, Kerala, India*
*Corresponding Author e-mail: §ramabadrancd@christcollegeijk.edu.in; *e-mail: sudheersebastian@christcollegeijk.edu.in*
Received May 9, 2025; revised July 11, 2025; accepted July 17, 2025

A simulation study utilizing SCAPS 1-D software was conducted to explore the effects of an additional P3HT (Poly 3-hexylthiophene) layer on the performance of bulk heterojunction polymer solar cells, specifically with the active layer P3HT: $IC_{60}BA$. The investigated cell structure is ITO/PEDOT:PSS/P3HT/P3HT:$IC_{60}BA$/ZnO NPs/Al. Following the standardization of the software, we determined the optimal parameters of the solar cell structure by analyzing various factors influencing cell performance across different layers. Subsequently, after optimizing the structure, the power conversion efficiency (PCE) improved significantly, rising from 5.18% without additional layer to 15.26% with additional layer.
Keywords: *Bulk heterojunction polymer solar cell; Fullerene; SCAPS 1-D; Active Layer; ETL; HTL*
PACS: 84.60.Jt; 81.05.Lg; 07.05.Tp

1. INTRODUCTION

A polymer solar cell (PSC) is an organic solar cell that utilizes polymers as the primary component for converting sunlight into electrical energy. The operation of PSCs relies on photoinduced charge transfer between a donor (the polymer) and an acceptor, typically a fullerene derivative. When exposed to sunlight, excitons are generated within the polymer, which then separate into electrons and holes at the donor-acceptor interface. These charge carriers are subsequently collected at the electrodes, producing an electric current. Key characteristics of PSCs include their ease of fabrication, adaptability, and low production costs. Additionally, they can be made partially transparent. However, a significant limitation is their relatively low power conversion efficiency (PCE), comparable to that of traditional silicon solar cells. While PSCs hold environmental advantages, they often exhibit lower stability and increased susceptibility to environmental changes.

Polymer solar cells (PSCs) can be broadly categorized into four main types: tandem PSCs, bulk heterojunction PSCs (the most prevalent and favored type), single-layer PSCs, and bilayer PSCs. These solar cells find applications in wearable technology, portable electronics, integrated photovoltaics, and energy harvesting for the Internet of Things. One of the key materials used in bulk heterojunction (BHJ) polymer solar cells is poly(3-hexylthiophene) (P3HT), which is notable for its high hole mobility, environmental stability, and extended absorption in the red region. Consequently, [6,6]-phenyl-C61-butyric acid methyl ester (PCBM), a soluble C60 derivative, has emerged as one of the most widely utilized organic semiconductors for acting as an electron acceptor [1-3]. P3HT:PCBM solar cells have demonstrated an open circuit voltage (Voc) of approximately 0.6 V [4], attributed to the low LUMO energy levels of PCBM, which is around -3.8 eV. In 2009, a novel C60 derivative named indene-C60 bisadduct ($IC_{60}BA$) was introduced, and due to its higher LUMO energy levels of approximately -3.74 eV, $IC_{60}BA$ has increasingly replaced PCBM as the preferred acceptor material in these solar cells [14]. This substitution has resulted in improved efficiencies and a higher Voc of about 0.84 V [5-9]

Bulk heterojunction organic solar cells (OSCs), in which the donor and acceptor materials are combined to form the active layer, were first proposed by Yu et al. in 1995. Since the introduction of this bulk heterojunction (BHJ) structure, the power conversion efficiency (PCE) of BHJ OSCs has significantly improved, rendering it a promising technology. Heeger and colleagues [10] were the first to utilize the BHJ structure for polymer-fullerene blends. Subsequent research revealed that increasing the diameters of the donor and acceptor domains through various additive techniques leads to enhanced performance [11,12]. In an effort to improve results and address the limitations associated with the poly(3-hexylthiophene) and [6,6]-phenyl-C61-butyric acid methyl ester (P3HT:PCBM) blend, which exhibits a relatively low open-circuit voltage (Voc) of 0.6 V, Li et al. demonstrated the use of indene-C60 bisadduct ($IC_{60}BA$) as an electron acceptor in BHJ PSCs [13]. This P3HT:$IC_{60}BA$ combination resulted in higher PCE values and an increased Voc of approximately 0.84 V [14,15]

In this study, the solar cell comprised of P3HT:$IC_{60}BA$ (poly(3-hexylthiophene): (indene-C60 bisadduct) was simulated using SCAPS 1-D Software [16]. The simulation software was standardized by comparing the simulated output with experimental data [17]. In the numerical simulation of the polymer solar cell (PSC), the hole transport layer (HTL) is represented by PEDOT:PSS, the active layer by the fullerene blend P3HT: $IC_{60}BA$, and the electron transport layer (ETL) by ZnO nanoparticles (ZnONPs). Aluminum (Al) and indium tin oxide (ITO) serve as the electrode materials in

Cite as: C.D. Ramabadran, K.S. Sudheer, East Eur. J. Phys. 3, 454 (2025), https://doi.org/10.26565/2312-4334-2025-3-50

this structure. The performance of a polymer solar cell with P3HT: $IC_{60}BA$ as the active layer is improved when P3HT is added as an extra layer. Based on previous investigations, the operational performance and efficiency of the device were augmented to 26.5% through the incorporation of an ultrathin P3HT polymeric layer serving as an interfacial medium between the hole transport material and the perovskite layer [18]. In order to effectively separate and collect charges, P3HT helps to increase the mobility of electrons and holes, which adds to improved charge transport qualities. It assists in maximizing the open-circuit voltage and current density by maximizing energy level alignment at the heterojunction interface [19,20]. P3HT can improve the active layer's structural ordering and crystallinity, resulting in bigger crystal domain sizes that strengthen the interpenetrating network necessary for efficient charge transfer [17]. Furthermore, P3HT's solubility in common solvents makes it possible to use simple solution-processing processes, which increases the layers' scalability and compatibility with a range of production methods [21]. All things considered, these characteristics help the solar cells' power conversion efficiency to rise noticeably. To the best of our knowledge, this is the first simulation study reporting the impact of using P3HT on Polymer solar cell with P3HT:$IC_{60}BA$ as active layer. In this simulation, we specifically investigated the impact of adding P3HT layer to the structure above.

2. DEVICE SIMULATION METHODOLOGY

The one-dimensional Solar Cell Capacitance Simulator (SCAPS) version 3.3.08 was employed as the numerical simulation tool in this investigation. This software is capable of solving both optical and electrical models throughout the entire configuration. We utilized a 1.5 AM spectrum for illumination. Previous simulations have focused on various types of solar cells, including perovskite, fullerene, non-fullerene bulk heterojunction (BHJ), and tandem solar cells (Abdelaziz et al., 2019, 2020; Gupta and Dixit, 2018; Bahrami et al., 2019). The application allows users to modify parameters and select the desired output across its various panels. Additionally, the software numerically solves Burgelman et al.'s generic semiconductor equations to obtain a steady-state operating point solution [16]

Equations foundational to semiconductors, including the Poisson equation, continuity equations, drift equations, and diffusion current equations, are used to efficiently evaluate the electrical performance of electronic devices when stimulated. The stimulation can take the form of heat energy, photons, or voltages. This indicates that we can compute the electrical performance of the devices and analyze their I-V characteristics using these equations. Consequently, these equations provide a theoretical basis for interpreting and assessing the measured performance of the devices. Furthermore, they can be employed to reduce experimental labor costs and to evaluate and predict the performance of new device structures, potentially leading to significant savings in both time and money.

They can be applied to streamline mathematical analysis and determine the ideal device structure parameters. The local microscopic behaviour of the material is described by these differential equations. The local electric field change resulting from the volumetric charge density at a particular location within a material is described by the Poisson equation [Equation 1]. The conservation of electrons and holes at a specific place in the material is expressed by the continuity equations [Equation 2]. In this instance, an electric field (drift current) or a concentration gradient (diffusion current) is driving the electron and hole currents [Equations 4-5]. [22]

$$\frac{\partial \varepsilon_0 \varepsilon}{\partial x}\frac{\partial \Psi}{\partial x} = -q\left(p - n + N_D - N_A + \frac{\rho_{def}}{q}\right), \tag{1}$$

$$-\frac{\partial J_n}{\partial x} - Un + G = \frac{\partial n}{\partial t}, \tag{2}$$

$$-\frac{\partial J_p}{\partial x} - Up + G = \frac{\partial p}{\partial t}, \tag{3}$$

$$Jn = -\frac{\mu_n n}{q}\frac{\partial E_{Fn}}{\partial x}, \tag{4}$$

$$Jp = +\frac{\mu_p p}{q}\frac{\partial E_{Fp}}{\partial x}. \tag{5}$$

In the abovementioned equations, the charge is denoted by q, and the electrostatic potential is denoted by Ψ. The symbols p, n, stand for free holes and electrons, respectively. Ionised donor-like and ionised acceptor-like doping concentrations are denoted by N_D and N_A. Here, ϵ signifies absolute permittivity, while ϵ_0 denotes permittivity in free space. The terms Jn and Jp signify electron and hole current densities, respectively, whereas Un denotes electron recombination rate. G is the generation rate, while Up is the rate of hole recombination. In contrast to what has been described so far, E_{Fn} and E_{Fp} stand for the electron and hole quasi-Fermi levels, whereas n and p indicate the electron and hole mobility, respectively

The glass substrate/ITO/PEDOT: PSS/P3HT:$IC_{60}BA$/ZnONPS/Al simulated bulk heterojunction structure is shown in Figure 1. The simulation's material properties, such as electron affinity (χ), bandgap energy (Eg), and relative permittivity (ε_r), are displayed in Table 1. Hole and electron mobilities are μp and μn, respectively. Donor and acceptor densities are denoted by N_D and N_A, respectively. The effective densities of states in the valence and conduction bands are denoted by Nv and Nc, respectively, while the defect density is represented by Nt. 4.8 and 4.2 eV are the settings for the anode and cathode work functions, respectively. The capture cross section for holes and electrons is set to 1×10^{-25} cm^2 across all layers, and the thermal velocity is set to 10^7 cm/s.

The four primary output parameters of a solar cell are power conversion efficiency (PCE), fill factor (FF), short circuit current (Jsc), and open circuit voltage (Voc). The necessary material parameters for simulation and absorption spectra have been compiled from the literature [16,17, 21–35]. A comparison analysis of the simulated and experimental data for SCAPS 1-D calibration is presented in Table 2. Additionally, Figure 2 illustrates the simulated polymer solar cell structure with additional P3HT layer.

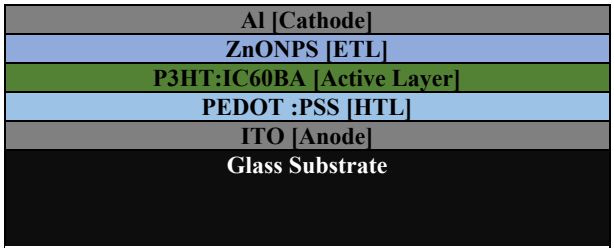

Figure 1. Simulated Bulk Heterojunction Polymer Solar Cell Structure for Standardization of SCAPS 1D

Table 1. Simulation parameters of Bulk Heterojunction Polymer Solar Cell

Parameters	HTL	Active Layer	ETL
Thickness [nm]	27	250	46
Eg (eV)	1.6	1.68	3.2
χ (eV)	3.4	3.880	4.6
ε_r	3.0	3.3	9.0
μ_n cm^2/vs	10	10^7	10^7
μ_p cm^2/vs	400	10^7	10^7
N_A (cm^{-3})	10^{15}	0	0
N_D (cm^{-3})	0	3.2×10^{18}	1.1×10^{18}
N_C (cm^{-3})	2.2×10^{15}	1.6×10^{20}	2.2×10^{19}
N_V (cm^{-3})	1.8×10^{18}	10^{19}	1.8×10^{19}
N_t (cm^{-3})	10^{15}	10^{16}	10^{15}

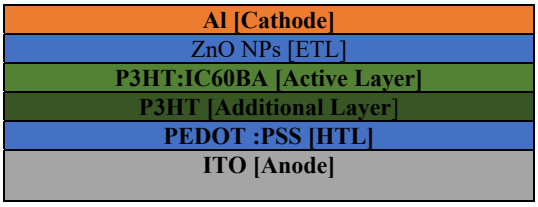

Figure 2. Simulated Polymer Solar Cell Structure

Table 2. Comparison of simulated parameterswith experimental results

Parameters	Experimental	Simulated
Voc (V)	0.84	0.85
Jsc(mA/cm^2)	8.36	8.21
FF(%)	59	57
PCE(%)	4.1	3.97

3. RESULTS AND DISCUSSION

We will analyze the solar cell structure shown in Figure 2 in greater detail. Each layer of the structure is examined to determine its performance under various parameters for optimal results. To achieve these optimal outcomes, new device structures are developed and their performance is thoroughly investigated. The following section provides an explanation of the simulation studies that were conducted.

3.1 Effect of Active Layer thickness

The thickness of the active layer is varied between 100 and 300 nm to assess the characteristics related to solar cell performance. The parameters Voc, Jsc, FF, and PCE demonstrate similar trends, with all reaching their optimal values at a thickness of 300 nm. These improvements at the ideal thickness can be attributed to reduced recombination and enhanced light absorption. Increasing the active layer thickness may enhance Jsc by allowing more light to be absorbed. However, this relationship is nonlinear; beyond an optimal thickness, it is affected by increased charge recombination and decreased charge transport efficiency, leading to diminishing returns [36, 37]. While Voc is not directly influenced by the thickness of the active layer, it is primarily determined by the energy levels of the donor and acceptor materials.

Nevertheless, recombination dynamics and the quality of the interface may play significant roles in its behavior [38, 39]. Certain experiments have demonstrated that increasing the thickness of the active layer can improve the power conversion efficiency (PCE) to a certain extent. The relevant graph is presented in Figure 3.

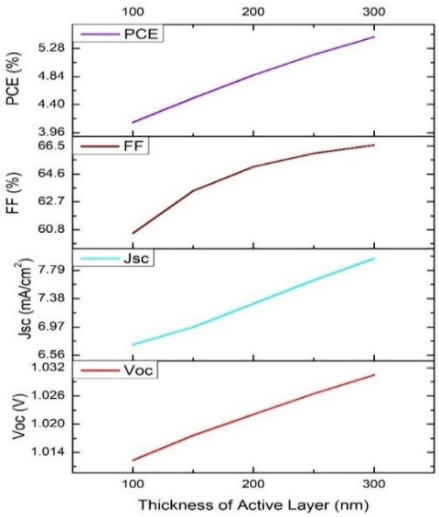

Figure 3. Influence of Active Layer Thickness

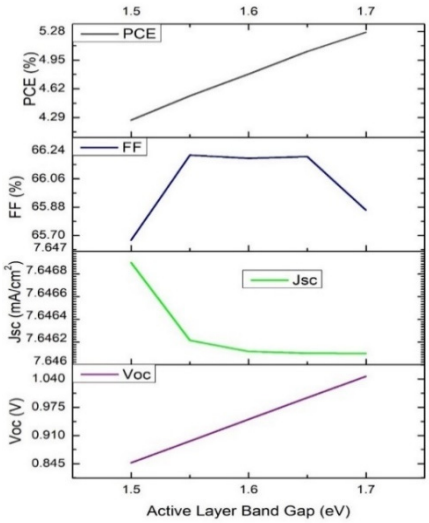

Figure 4. Influence of Active Layer Bandgap

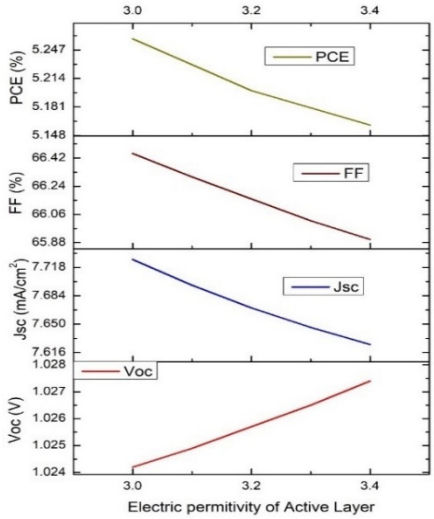

Figure 5. Influence of Electric Permittivity of Active Layer

3.2 Influence of Active Layer Band Gap

The active layer band gap is varied from 1.5 eV to 1.7 eV, and both power conversion efficiency (PCE) and open-circuit voltage (Voc) exhibit similar variations with bandgap. Both PCE and Voc reach their maximum at 1.7 eV. In organic solar cells, Voc is determined by the difference between the lowest unoccupied molecular orbital (LUMO) of the acceptor material and the highest occupied molecular orbital (HOMO) of the donor material. As the bandgap of the active layer increases, the Voc tends to increase as well, reflecting either a higher LUMO level of the donor or a lower HOMO level of the acceptor. This relationship is influenced by the energy levels of the donor and acceptor materials, which impact Voc in connection with the difference between the quasi-Fermi levels of the electrons and holes. A larger bandgap reduces the energy loss between the bandgap energy (Eg) and Voc. However, in organic solar cells, the Voc is generally lower than the bandgap energy due to non-radiative recombination and other losses. As the bandgap increases, Voc approaches Eg, resulting in an overall increase in Voc. Furthermore, the power conversion efficiency of a solar cell is calculated by multiplying its fill factor (FF), open-circuit voltage (Voc), and short-circuit current (Jsc).

As mentioned earlier, an increase in the bandgap can lead to a higher open-circuit voltage (Voc), which may subsequently enhance the power conversion efficiency (PCE). However, a wider bandgap often results in reduced solar spectrum absorption by the solar cell, particularly in the infrared region, which can lower the short-circuit current (Jsc). Nevertheless, in some cases, the increase in Voc associated with a wider bandgap can compensate for the decrease in Jsc, resulting in an overall increase in PCE. Additionally, the fill factor (FF) may improve with an increasing bandgap due to enhanced charge carrier transfer [40], although this trend is not always consistent. With further increases in bandgap, FF may remain stable or even decline, possibly due to the effects of recombination processes and exciton lifetimes [41, 42]. The relationship between FF and bandgap is complex and depends on the specific materials and cell architecture used in the organic solar cell. The relevant graph illustrating these dynamics is presented in Figure 4.

3.3 Effect of Electric Permittivity of Active Layer

In this section, we have analyzed the impact of the active layer's electric permittivity [ε] on the performance of the polymer solar cell. The electric permittivity is varied from 3.0 to 3.4. The findings indicate that while the open-circuit voltage (Voc) increases with ε, all other parameters are found to decrease. The electric permittivity of the active layer influences the dielectric properties of the material, which in turn affects the open-circuit voltage of polymer solar cells (PSCs). Consequently, a higher electric permittivity in the active layer may lead to an increase in Voc due to its effect on the dynamics of charge carriers within the solar cell.

A higher electric permittivity enhances charge carrier separation and reduces recombination losses by decreasing the Coulombic interaction between charge carriers [43]. This improvement can result in a stronger built-in electric field and more efficient charge extraction, both of which contribute to an increased open-circuit voltage (Voc). However, optimizing the performance of polymer solar cells (PSCs) requires a comprehensive understanding

of all contributing parameters, as a higher permittivity can indeed enhance Voc. The electric permittivity of the active layer also influences the short-circuit current (Jsc), fill factor (FF), and power conversion efficiency (PCE) of PSCs by affecting the dissociation of photogenerated electron-hole pairs and the movement of charge carriers within the device. Elevated Coulombic attraction between opposing charges can occur with high electric permittivity, potentially hindering their separation and reducing Jsc [44]. Additionally, a larger permittivity may negatively impact charge carrier mobility, leading to increased recombination rates and declines in both FF and PCE. The relevant graph illustrating these relationships is presented in Figure 5.

3.4: Effect of Conduction Band Density of States of Active Layer

In this section, we examine how varying the conduction band density of states in the active layer from 1.6×10^{19} to 1.6×10^{21} cm^{-3} affects the performance metrics of polymer solar cells. Figure 6 illustrates the corresponding data. The graph indicates that while short-circuit current (Jsc) and power conversion efficiency (PCE) fluctuate similarly, the open-circuit voltage (Voc) and fill factor (FF) do not exhibit the same trend. The decline in Voc with an increase in the conduction band density of states in the active layer is primarily attributed to enhanced recombination losses and shifts in the Fermi level.

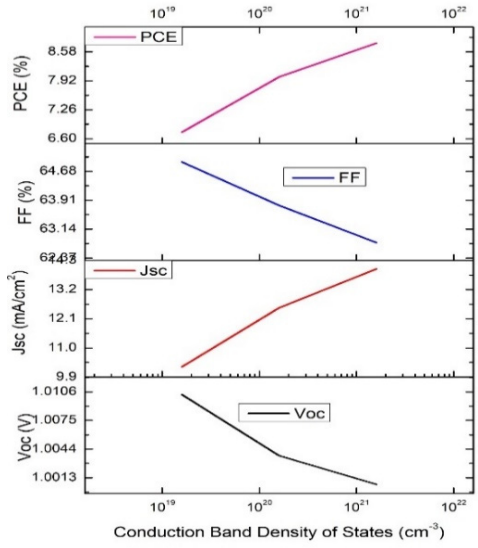

Figure 6. Influence of CB density of states of Active Layer

Recombination events are more likely to occur when the density of states is higher, as this provides more energy levels for charge carriers to occupy [45]. The increase in short-circuit current density (Jsc) associated with a higher conduction band density of states (DOS) in the active layer can be attributed to increased charge carrier generation and improved collection efficiency. A greater DOS enhances the availability of conduction states, leading to more efficient photon absorption and, consequently, a higher production of electron-hole pairs. This directly correlates with an increase in Jsc [46]. However, the rise in power conversion efficiency (PCE) and the decline in fill factor (FF) of polymer solar cells with an increasing conduction band DOS result from a combination of enhanced charge generation and increased recombination losses. While a higher DOS contributes to improved charge carrier absorption and generation, it also results in more opportunities for recombination, which negatively impacts the FF [45].

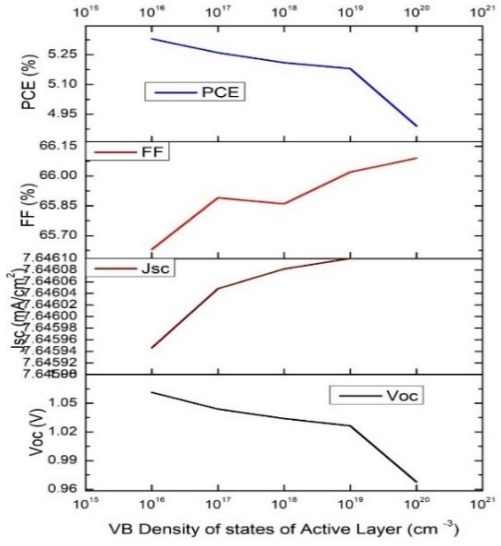

Figure 7. Influence of VB density of states of Active Layer

3.5 Effect of Valence Band Density of States of Active Layer

The valence band density of states in the active layer is varied from 1×10^{16} to 1×10^{20} cm^{-3}, and its impact on the characteristics of polymer solar cells is evaluated. The analysis reveals that while short-circuit current density (Jsc) and fill factor (FF) change in a similar manner, open-circuit voltage (Voc) and power conversion efficiency (PCE) do not exhibit the same trend. The decline in PCE and Voc with an increase in valence band density of states (DOS) is primarily due to enhanced recombination rates and increased charge carrier trapping. Although a higher valence band DOS might initially seem beneficial, it generates more energy states that facilitate non-radiative recombination processes and hinder charge transport, which adversely affects both PCE and Voc [47-48]. Figure 7 shows the respective graph.

3.6. Effect of Shallow Uniform Density of States of Active Layer

The shallow uniform density of states in the active layer experiences a significant shift from 3.2×10^{14} to 3.2×10^{16} cm^{-3}. As this density increases, parameters such as open-circuit voltage (Voc), fill factor (FF), and power conversion efficiency (PCE) tend to improve, while the short-circuit current (Jsc) shows a decline. An elevated donor density can enhance the intrinsic potential across the junction by increasing the availability of charge carriers. This rise in potential positively impacts Voc, which is crucial for the efficient operation of solar cells, as it reduces losses during charge separation. Furthermore, an increase in donor density leads to enhanced conductivity within the active layer, which

in turn lowers series resistance. This reduction in series resistance facilitates a higher fill factor by minimizing voltage drops during operation [49]. The graphical representation is given in Figure 8. However, a noticeable increase in shallow donor density can also result in a higher defect density within the active layer. This heightened defect density may give rise to additional recombination centers that foster nonradiative recombination of charge carriers. Consequently, this adverse effect results in fewer charge carriers contributing to the photocurrent, thereby reducing the short-circuit current [50].

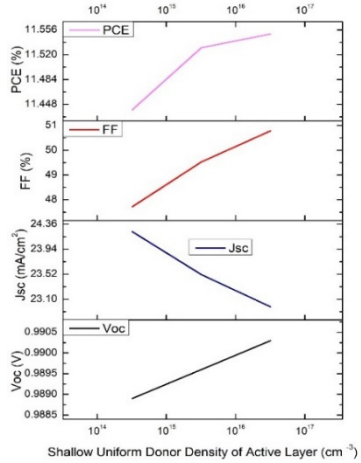

Figure 8. Influence of Shallow Uniform Donor Density of states of Active Layer

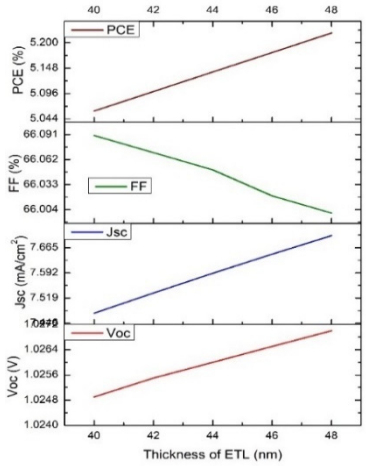

Figure 9. Influence of ETL Thickness

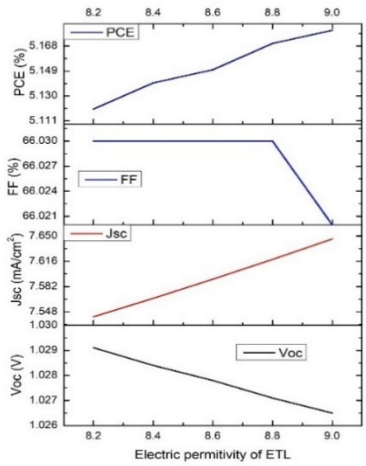

Figure 10. Effect of Electric Permitivity of ETL

3.7. Effect of Thickness of ETL

This study examines the effect of varying the thickness of the electron transport layer (ETL) made from zinc oxide nanoparticles (ZnONPs), changing it from 40 nm to 48 nm. The optimal performance was identified at a thickness of 48 nm, where the power conversion efficiency (PCE) peaked at 5.22%, the open circuit voltage (Voc) reached 1.0270 V, and the short-circuit current density (Jsc) was measured at 7.699979 mA/cm². At 40 nm thickness, the fill factor (FF) was observed to achieve a higher value of 66.09%. The analysis of output parameters indicates that as the thickness increases, the fill factor tends to decrease, while Voc, Jsc, and PCE show an upward trend. Thicker ETLs can enhance the open circuit voltage (Voc) in polymer solar cells by slowing down charge recombination processes. By expanding the electron transport pathway, a thicker ETL minimizes the likelihood of electron-hole recombination before charge carriers reach the electrodes. This increased thickness facilitates a more effective collection of photo-generated electrons due to the greater transit space afforded to the electrons. Consequently, as more charge carriers efficiently reach the electrodes with minimal losses from trapping or recombination, this improvement in charge transport can lead to higher Jsc [51]. However, the decline in the fill factor in polymer solar cells at greater ETL thicknesses is primarily attributed to increased series resistance, reduced charge carrier mobility, elevated recombination rates, and interfacial charge transfer resistance [52]. The power conversion efficiency (PCE) of polymer solar cells can improve with increased thickness of the ETL, up to a certain optimal point, largely due to better light absorption, enhanced charge extraction, and superior charge transport capabilities [53]. The respective graph is shown in Figure 9.

3.8 Effect of Electric Permitivity of ETL

This section provides a comprehensive analysis of how the electric permittivity of the electron transport layer (ETL) affects polymer solar cells, as illustrated in Figure 10. The findings reveal that changing the electric permittivity from 8.2 to 9.0 results in a decrease in the open-circuit voltage (Voc), while both the short-circuit current density (Jsc) and overall efficiency experience an increase. Specifically, a permittivity value of 9.0 yields the best optimized performance. For effective charge transfer, the energy levels of the ETL and the active layer must be closely aligned. Higher permittivity in the ETL may disrupt this alignment at the ETL/polymer interface, leading to voltage loss and a reduction in Voc due to ineffective charge transfer. Quality issues within the ETL can further diminish Voc and impede charge transfer, even if the permittivity is elevated. Since successful charge collection relies on the interactions between charge carriers and their respective layers, any adverse effects on the electrostatic potential exacerbated by materials with high dielectric constants [54] can contribute to a lower Voc. Conversely, increased electric permittivity facilitates faster charge transfer at the donor-acceptor interface, significantly reducing non-geminate recombination losses. By minimizing these losses, more charge carriers become available for collection, enhancing the overall performance of the solar cell.

Ultimately, improved charge dynamics and reduced recombination lead to higher values of Jsc and power conversion efficiency (PCE), which can be attributed to a favourable dielectric environment [55]. However, flaws or suboptimal interfaces can still generate recombination losses, which may diminish the fill factor's responsiveness to changes in permittivity.

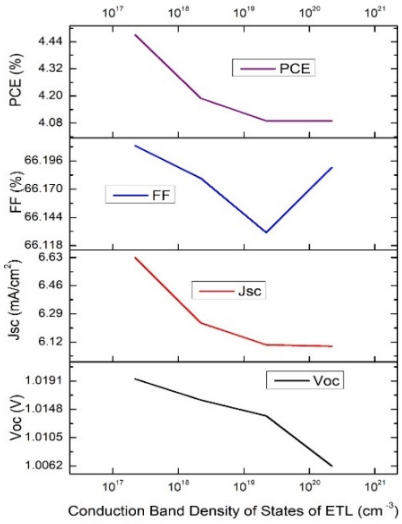

Figure 11. Influence of Conduction Band Density of States of ETL

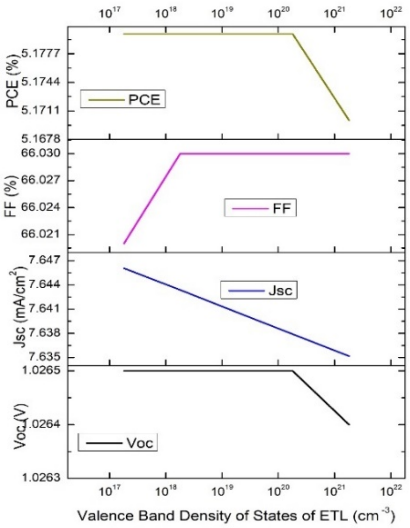

Figure 12. Influence of Valence Band Density of States of ETL

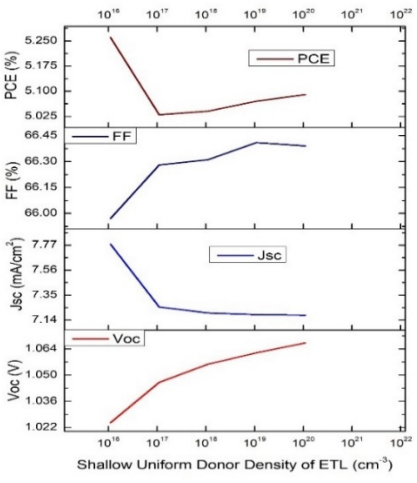

Figure 13. Influence of Shallow Donor Density of ETL

3.9 Effect of Conduction Band Density of States of ETL

This section investigates the influence of the conduction band density of states (CBDoS) of a polymer cell on the performance of its electron transport layer (ETL). For this analysis, the CBDoS is varied from 2.2×10^{17} to 2.2×10^{20} cm^{-3}. It was observed that the short-circuit current density (Jsc) and power conversion efficiency (PCE) exhibited similar trends, while the fill factor (FF) initially decreased before increasing at higher CBDoS values. The performance was found to be optimized at 2.2×10^{17} cm^{-3}, as illustrated in Figure 11. The decline in Jsc and PCE with increasing CBDoS is primarily attributed to increased carrier trapping, higher recombination rates, and potential misalignment of energy levels [56]. As the CBDoS rises, the presence of additional trap states hinders charge extraction and facilitates enhanced carrier recombination, leading to a reduction in open-circuit voltage (Voc). The behaviour of the fill factor (FF) is influenced by the complex interactions among energy level alignment, trap states, and carrier dynamics. This results in a non-linear relationship, where the competing effects of increased recombination and improved carrier mobility contribute to the observed patterns in FF.

3.10 Effect of Valence Band Density of States of ETL

This section focuses on the changes in the valence band density of states of the electron transport layer in polymer solar cells, varying from 1.8×10^{17} to $1.8\times10^{21}cm^{-3}$. Figure 12 provides a graphical representation of these changes.

It was found that the optimal performance, characterized by a maximum efficiency of 5.18%, occurs at a density of $1.8x10^{17}$ cm^{-3}. Variations in the valence band density of states within the electron transport layer can lead to complex changes in the output characteristics of polymer solar cells. The effects on short-circuit current density (Jsc), open-circuit voltage (Voc), fill factor (FF), and power conversion efficiency (PCE) are determined by optimizing the density of states, alongside the ratio of charge transport to recombination and the alignment of interfacial energy levels. The respective graph is given in Figure 12.

3.11 Effect of Shallow Donor Density of ETL

This section analyzes the fluctuations in the shallow donor density of the electron transport layer, which ranges from 1.1×10^{16} to 1.1×10^{20} cm^{-3}. Figure 13 provides the corresponding graph illustrating these fluctuations. The findings indicate that while the variations in short-circuit current density (Jsc) and power conversion efficiency (PCE) are comparable, the changes in open-circuit voltage (Voc) and fill factor (FF) exhibit a similar trend. Voc typically increases with a higher shallow donor density, as this leads to improved charge extraction and reduced recombination losses. Additionally, as charge transport and extraction enhance, the fill factor (FF) also rises with the shallow donor density. However, excessive concentrations of shallow donors can lead to significant recombination, ultimately resulting in a decrease in PCE.

3.12 Effect of Thickness of Additional P3HT Layer

In this case, the thickness of the P3HT layer is varied from 16 nm to 24 nm, with the optimal performance observed at 16 nm.

This is illustrated in Figure 14, which provides a graphical representation of the findings. The investigation reveals that while the fill factor (FF) shows a different trend, the open-circuit voltage (Voc), short-circuit current density (Jsc), and power conversion efficiency (PCE) fluctuate similarly. As the P3HT layer increases in thickness, the pathways for charge transport become longer and more convoluted.

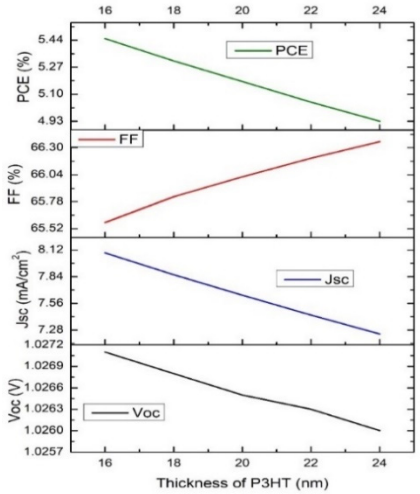

Figure 14. Influence of P3HT Thickness

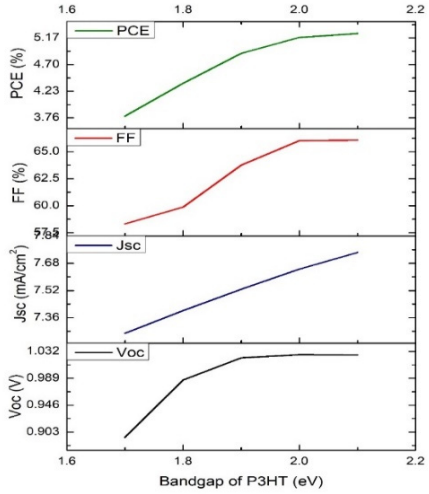

Figure 15. Effect of Band gap of P3HT

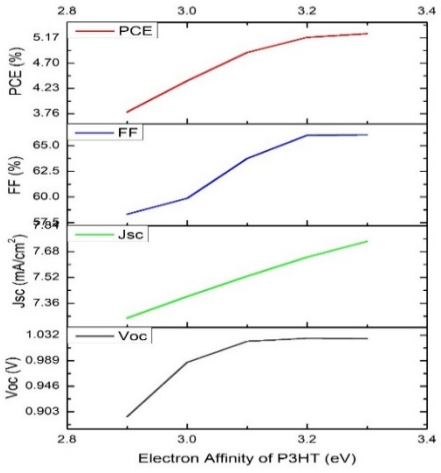

Figure 16. Influence of Electron Affinity of P3HT

Consequently, charge carrier mobility diminishes, which is crucial for the effective transfer of electrons and holes to their respective electrodes. This increase in the distance that charge carriers must traverse can lead to a higher likelihood of recombination before reaching the electrodes, potentially resulting in reduced Jsc and PCE. Moreover, the drop in Voc may be attributed to lower charge extraction efficiency in thicker layers and higher energy losses associated with elevated recombination rates. Key factors contributing to the decline in FF in polymer solar cells (PSCs) as the P3HT layer thickness increases include enhanced bimolecular recombination, inefficient charge transport, and imbalanced charge carrier mobilities [57].

3.13. Effect of Bandgap of Additional P3HT Layer

The bandgap of P3HT varies from 1.7 eV to 2.1 eV, with observations indicating that all output parameters increase alongside the bandgap. This trend is illustrated in Figure 15. There is a direct correlation between the open-circuit voltage (Voc) and the energy levels of the polymer's lowest unoccupied molecular orbital (LUMO) and highest occupied molecular orbital (HOMO). Generally, a larger bandgap ensures a higher HOMO energy level, which can enhance Voc. Additionally, higher bandgap materials are more effective at absorbing high-energy photons, potentially leading to increased short-circuit current density (Jsc). Increasing the bandgap creates a larger energy difference necessary for charge separation, which reduces the likelihood of exciton recombination. This mechanism ultimately contributes to an improvement in both fill factor (FF) and power conversion efficiency (PCE).

3.14 Effect of Electron Affinity of Additional P3HT Layer

This section investigates the influence of P3HT's electron affinity on the performance of polymer solar cells. The electron affinity is varied from 2.9 eV to 3.3 eV, revealing that all output parameters of the cell respond similarly to these changes. Figure 16 illustrates this correlation. In general, a higher electron affinity results in an elevated LUMO energy level, which can lead to an increase in the open-circuit voltage (Voc) when no current is flowing. Larger electron affinities create greater energy offsets, facilitating the efficient movement of electrons and potentially enhancing the short-circuit current density (Jsc). Furthermore, a polymer donor with a higher electron affinity can reduce recombination losses, leading to improved fill factor (FF) and power conversion efficiency (PCE) [58].

3.15 Effect of Valence Band Density of States of Additional P3HT Layer

The present study investigates the effect of varying the valence band density of states of P3HT from 1.8×10^{16} to 1.8×10^{20} cm^{-3} on the output parameters of polymer solar cells. While the short-circuit current density (Jsc) shows a differential response among the output parameters, the open-circuit voltage (Voc), fill factor (FF), and power conversion efficiency (PCE) exhibit similar trends. This relationship is illustrated in Figure 17.

Improvements in metrics such as PCE, FF, and Voc can be attributed to better energy level alignment and enhanced charge transport. However, as the valence band density increases, performance declines due to higher defect densities and shorter diffusion lengths, ultimately reducing the overall efficiency of the solar cell. The maximum efficiency is observed at a valence band density of 1.8×10^{17} cm^{-3}. The decrease in Jsc for polymer solar

cells, particularly those utilizing P3HT, is primarily caused by increased defect density and shorter charge carrier diffusion lengths associated with high density states.

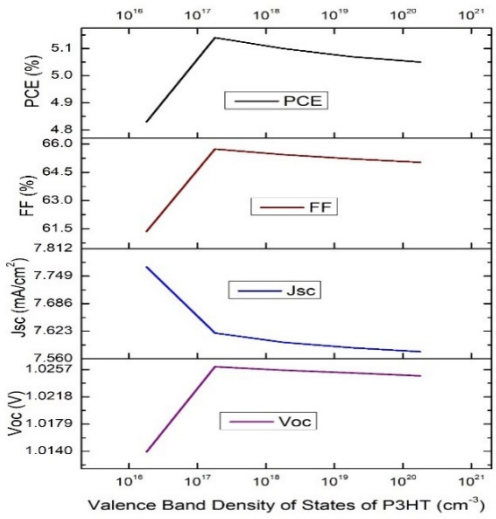

Figure 17. Influence of Valence Band Density of States of P3HT

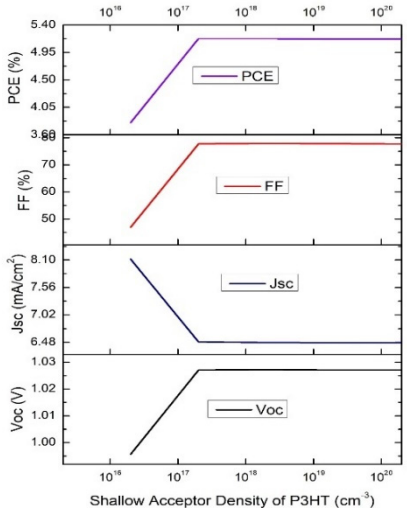

Figure 18. Influence of Shallow Acceptor Density of States of P3HT

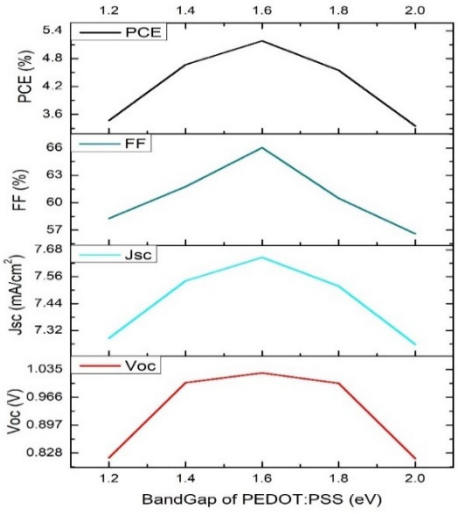

Figure 19. Influence of Bandgap of PEDOT : PSS

3.16 Effect of Shallow Acceptor Density of States of Additional P3HT Layer

In our subsequent endeavor, we adjusted the shallow acceptor density of states in the P3HT layer, conducting a study that encompassed values ranging from 2×10^{16} to 2×10^{20} cm^{-3}. The optimal performance was observed at a density of 2×10^{17} cm^{-3}, as illustrated in Figure 18, which displays the graphical variations. The fluctuations in performance were similar to those seen with the layer's valence band density of states. This similarity arises because both factors significantly influence the solar cell's charge transport, carrier density, trap formation, and recombination dynamics. The sensitivity of performance to these concentrations highlights the delicate balance required to enhance charge mobility while minimizing the adverse effects of defects.

3.17 Effect of Bandgap of PEDOT: PSS [HTL]

This study investigates the impact of changing the bandgap of the hole transport layer, PEDOT:PSS, from 1.2 eV to 2.0 eV on the output parameters of polymer solar cells. All parameters were observed to fluctuate similarly, with maximum efficiency achieved at a bandgap of 1.6 eV, as illustrated in Figure 19. Increasing the PEDOT:PSS bandgap can enhance the open-circuit voltage (Voc) in polymer solar cells. However, a higher bandgap limits sunlight absorption, resulting in lower charge carrier production. Due to the significantly high bandgap of PEDOT:PSS, sunlight absorption is reduced, which subsequently decreases the short-circuit current density (Jsc). Additionally, the hydrophilic nature and instability of the hole transport layer (HTL) may lead to increased series resistance, further affecting the fill factor (FF). The power conversion efficiency (PCE) increases initially but subsequently declines as the hole transport bandgap is raised.

3.18 Effect Electron Affinity of PEDOT:PSS [HTL]

PEDOT:PSS demonstrates a shift in electron affinity ranging from 3.0 eV to 3.8 eV, with optimized values achieved at 3.4 eV, as illustrated in Figure 20. The output parameters of polymer solar cells exhibit similar changes as the bandgap and electron affinity of PEDOT:PSS are increased. This similarity arises from the interplay between energy level alignment and charge transport dynamics, both of which are simultaneously influenced by these two characteristics.

CONCLUSION

In this modeling work, a P3HT layer was integrated into a polymer solar cell structure using SCAPS 1-D software, with P3HT:$IC_{60}BA$ serving as the active layer. The study revealed that the structure exhibited significantly better performance with the inclusion of P3HT. The P3HT layer enhances charge transit and maximizes Voc and Jsc by aligning energy levels at the heterojunction surfaces. After optimization, the following output parameters were achieved: power conversion efficiency (PCE) = 15.26%, fill factor

(FF) = 51.62%, short-circuit current density (Jsc) = 26.577140 mA/cm², and open-circuit voltage (Voc) = 1.1126 V. Before optimization, we recorded an efficiency of only 5.18%. These results are quite promising and will contribute to the advancement of photovoltaic research in the future.

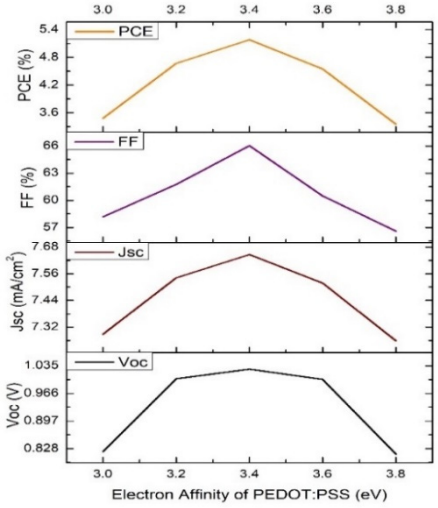

Figure 20. Influence of Electron Affinity of PEDOT: PSS

Statements and Declarations:

Data availability statement: The data that support the findings of this study are available on request from the corresponding author.

Acknowledgements. For providing SCAPS 1-D software for the simulation investigation, the authors would like to thank Pr.M. Burgelman of the University of Gent in Belgium.

CRediT authorship contribution statement.: Ramabadran C.D.: Conceptualization, Data curation, Methodology, Software, Investigation, Validation, Formal analysis, Writing – original draft. Sudheer K.S.: Supervision, Conceptualization, Software, Writing – review & editing

Conflict of interest. The authors declare that they have no conflict of interest.

ORCID

Chittur Devarajan Ramabadran, https://orcid.org/0009-0003-2255-3087; **K. Sebastian Sudheer,** https://orcid.org/0000-0002-9019-4405

REFERENCES

[1] Y. He, G. Zhao, B. Peng, and Y. Li, "High-Performance Polymer Solar Cells with P3HT:PCBM Bulk Heterojunction: A Combined Experimental and Simulation Study," Advanced Functional Materials, **20**(19), 3383–3389 (2010). https://doi.org/10.1002/adfm.201000973

[2] C. Bendenia, H. Merad-Dib, S. Bendenia, and B. Hadri, "Numerical simulation of CIGS solar cells with SCAPS-1D: Optimization of the absorber band gap grading and thickness," Optik, **174**, 167–172 (2018). https://doi.org/10.1016/j.ijleo.2018.08.058

[3] A. Hazra, I. Mal, D. Samajdar, and T. Das, "Device simulation of lead-free $CH_3NH_3SnI_3$ perovskite solar cells with high efficiency," Optik, **168**, 747–753 (2018). https://doi.org/10.1016/j.ijleo.2018.04.117

[4] Y. Sun, C. Cui, H. Wang, and Y. Li, "Fabrication of Flexible, Free-Standing, Ultralight Carbon Nanotube Aerogel Films for Supercapacitor Electrodes," Advanced Energy Materials, **1**(6), 1058–1061(2011). https://doi.org/10.1002/aenm.201100322

[5] Y. He, H.-Y. Chen, J. Hou, and Y. Li, "Indene−C60 Bisadduct: A New Acceptor for High-Performance Polymer Solar Cells," Journal of the American Chemical Society (JACS), **132**(4), 1377–1382 (2010). https://doi.org/10.1021/ja908602j

[6] G. Zhao, Y. He, and Y. Li, "6.5% Efficiency of Polymer Solar Cells Based on poly(3- hexylthiophene) and Indene-C60 Bisadduct by Device Optimization," Advanced Materials, **22**(39), 4355–4358 (2010). https://doi.org/10.1002/adma.201001339

[7] Z. Tan, D. Qian, W. Zhang, L. Li, Y. Ding, Q. Xu, F. Wang, and Y. Li, "Efficient and stable polymer solar cells with a solution-processable small molecule as anode buffer layer," Journal of Materials Chemistry A, **1**(3), 657–664 (2013). https://doi.org/10.1039/C2TA00575F

[8] S. Gartner, M. Christmann, S. Sankaran, H. Röhm, E.-M. Prinz, F. Penth, A. Pütz, *et al*., "esign Rules for High-Efficiency Polymer Solar Cells with Low Energy Loss and High Fill Factor," Advanced materials, **26**(38), 6653–6657 (2014). https://doi.org/10.1002/adma.201402932

[9] E.F. Oliveira, L.C. Silva, and F.C. Lavarda, "Electronic structure and charge transport properties of star-shaped molecules with 1,3,5-triazine core and thiophene arms for photovoltaic applications," Structural Chemistry, **28**, 1133–1140 (2017). https://doi.org/10.1007/s11224-017-0926-y

[10] G. Yu, J. Gao, J.C. Hummelen, F. Wudl, and A.J. Heeger, "Polymer Photovoltaic Cells: Enhanced Efficiencies via a Network of Internal Donor-Acceptor Heterojunctions," Science, **270**, 1789 -1791 (1995). https://doi.org/10.1126/science.270.5243.1789

[11] J. Peet, J.Y. Kim, N.E. Coates, W.L. Ma, D. Moses, A.J. Heeger, and G.C. Bazan, "Efficiency enhancement in low-bandgap polymer solar cells by processing with alkane dithiols," Nature materials, **6**(7), 497–500 (2007). https://doi.org/10.1038/nmat1928

[12] J.K. Lee, W.L. Ma, C.J. Brabec, J. Yuen, J.S. Moon, J.Y. Kim, K. Lee, *et al*., "Processing additives for improved efficiency from bulk heterojunction solar cells," Journal of the American Chemical Society, **130**(11), 3619–3623 (2008). https://doi.org/10.1021/ja710079w

[13] N. Loew, S. Komatsu, H. Akita, K. Funayama, T. Yuge, T. Fujiwara, and M. Ihara, "Development of a novel glucose sensor using engineered glucose dehydrogenase," ECS Transactions, **58**(45), 77- 82 (2014). https://doi.org/10.1149/05845.0077ecst
[14] P. Matavulj, M.K. Islam, and C.S. Živanović, "Numerical simulation of organic solar cells: Impact of interface layers on device performance," in: *Proceedings of the International Conference on Numerical Simulation of Optoelectronic Devices (NUSOD)*, (IEEE, Copenhagen, Denmark, 2017), pp. 133–134. https://doi.org/10.1109/NUSOD.2017.8010026
[15] S.-A. Gopalan, A.-I. Gopalan, A. Vinu, K.-P. Lee, and S.-W. Kang, "A new strategy for designing high-efficiency cascaded solar cells: Optical and electrical modeling using SCAPS-1D," Solar Energy Materials and Solar Cells, **174**, 112-123 (2018). https://doi.org/10.1016/j.solmat.2017.08.033
[16] M. Burgelman, P. Nollet, and S. Degrave, "Modelling polycrystalline semiconductor solar cells," Thin Solid Films, **361-362**, 527-532 (2000). https://doi.org/10.1016/S0040-6090(99)00825-1
[17] B. Xu, G. Sai-Anand, A.-I. Gopalan, Q. Qiao, and S.-W. Kang, "Improving Photovoltaic Properties of P3HT:$IC_{60}BA$ through the Incorporation of Small Molecules," Polymers, **10**(2), 121 (2018). https://doi.org/10.3390/polym10020121
[18] S. Hosseini, M. Bahramgour, N. Delibaş, and A. Niaie, "Investigation of a Perovskite Solar Cell and Various Parameters Impact on Its Layers and the Effect of Interface Modification by Using P3HT as an Ultrathin Polymeric Layer Through SCAPS-1D Simulation," Sakarya University Journal of Science, **25**(5), 1168-1179 (2021). https://doi.org/10.16984/saufenbilder.947735
[19] A. Maillard and A. Rochefort, "Quantum transport properties of graphene nanoribbons with embedded heptagon-pentagon defects," Organic Electronics, **15**(9), 2091-2098 (2014). https://doi.org/10.1016/j.orgel.2014.05.028
[20] H. Lee, (2015). "Optimization of energy level alignment for efficient organic photovoltaics," Vacuum Magazine, **2**(2), 12-16 (2015). https://doi.org/10.5757/VACMAG.2.2.12 (in Korean)
[21] S. Holliday, *et al*., "High-efficiency and air-stable P3HT solar cells with a new non-fullerene acceptor," Nature Communications, **7**, 11585 (2016). https://doi.org/10.1038/ncomms11585
[22] A. Kumar, and R. Singh, "Numerical Modelling Analysis for Carrier Concentration Level Optimization of CdTe Heterojunction Thin Film-Based Solar Cell with Different Non-Toxic Metal Chalcogenide Buffer Layers Replacements: Using SCAPS–1D Software," Crystals, **11**(12), 1454 (2021). https://doi.org/10.3390/cryst11121454
[23] K. Nithya, and K. Sudheer, "Numerical modelling of non-fullerene organic solar cell with high dielectric constant ITIC-OE acceptor," Journal of Physics Communications, **4**(2), 025012 (2020). https://doi.org/10.1088/2399-6528/ab772a
[24] S.W. Heo, E.J. Lee, K.W. Seong, and D.K. Moon, "Enhanced stability in polymer solar cells by controlling the electrode work function via modification of indium tin oxide," Solar energy materials and solar cells, **115**, 123–128, (2013). https://doi.org/10.1016/j.solmat.2013.03.023
[25] S. Loser, C.J. Bruns, H. Miyauchi, R.P. Ortiz, A. Facchetti, S.I. Stupp, and T.J. Marks, "A Naphthodithiophene-Diketopyrrolopyrrole Donor Molecule for Efficient Solution-Processed Solar Cells," Journal of the American Chemical Society, **133**(21), 8142– 8145 (2011). https://doi.org/10.1021/ja202791n
[26] G. Li, Y. Yao, H. Yang, V. Shrotriya, G. Yang, and Y. Yang, "Solvent annealing' effect in polymer solar cells based on poly(3-hexylthiophene) and methanofullerenes," Advanced Functional Materials, **17**(10), 1636–1644 (2007). https://doi.org/10.1002/adfm.200600624
[27] Z. He, F. Liu, C. Wang, J. Chen, L. He, D. Nordlund, H. Wu, T.P. Russell, and Y. Cao, "Simultaneous Enhancement of Open-Circuit Voltage, Short-Circuit Current Density, and Fill Factor in Polymer Solar Cells," Materials Horizons, **2**(6), 592–597(2015). https://doi.org/10.1039/C5MH00164A
[28] X. Zhu, K. Lu, B. Xia, J. Fang, Y. Zhao, T. Zhao, Z. Wei, *et al*., "Improving the Performances of Random Copolymer Based Organic Photovoltaics by Incorporating Fluorine Substituents," Polymers, **8**(1), 4 (2015). https://doi.org/10.3390/polym8010004
[29] L. Lu, *et al*., "High-performance ternary blend polymer solar cells involving both energy transfer and hole relay processes," Nat. Commun. **6**, 7327 (2015). https://doi.org/10.1038/ncomms8327
[30] M.M. Stylianakis, D. Konios, C. Petridis, G. Kakavelakis, E. Stratakis, and E. Kymakis, "Efficient and stable hybrid perovskite–graphene solar cells via interfacial passivation with 2D–2D heterostructures," 2D Materials, **4**(4), 042005 (2017). https://doi.org/10.1088/2053-1583/aa87b6
[31] B.N. Ezealigo, A.C. Nwanya, A. Simo, R.U. Osuji, R. Bucher, M. Maaza, and F.I. Ezema, "Optical and electrochemical capacitive properties of copper (I) iodide thin film deposited by SILAR method," Arabian Journal of Chemistry, **12**(8), 5380–5391 (2019). https://doi.org/10.1016/j.arabjc.2017.01.008
[32] J. Liu, Y. Zhang, C. Liu, M. Peng, A. Yu, J. Kou, W. Liu, *et al*., "High-Performance UV Photodetector Based on a Heterojunction of a ZnO Nanowire Array and a Few-Layer MoS_2 Film," Nanoscale research letters, **11**, 1–7 (2016). https://doi.org/10.1186/s11671-016-1291-2
[33] Z. El Jouad, M. Morsli, G. Louarn, L. Cattin, M. Addou, and J.C. Bern`ede, "Improving the efficiency of subphthalocyanine based planar organic solar cells through the use of MoO3/CuI double anode buffer layer," Solar Energy Materials and Solar Cells, **141**, 429– 435 (2015). https://doi.org/10.1016/j.solmat.2015.06.017
[34] M.I. Hossain, F.H. Alharbi, and N. Tabet, "Copper oxide as inorganic hole Transport material for lead halide perovskite based solar cells," Solar Energy, **120**, 370–380 (2015). https://doi.org/10.1016/j.solener.2015.07.037
[35] B.M. Omer, A. Khogali, and A. Pivrikas, "Combined effects of carriers charge mobility and electrodes work function on the performance of organic photovoltaic devices," in: *37th IEEE Photovoltaic Specialists Conference*, pp. 000734–000743 (IEEE, 2011). https://doi.org/10.1109/LED.2011.2117953
[36] O.D. Iakobson, O.L. Gribkova, A.R. Tameev, and J.-M. Nunzi, "Polymeric semiconductors for hybrid organic-inorganic solar cells: A comparative study of water-soluble polythiophenes," Scientific Reports, **11**, 3697 (2021). https://doi.org/10.1038/s41598-021-84452-x
[37] N. Sharma, S.K. Gupta, and C.M. Singh Negi, "Enhanced performance of organic solar cells by using zinc oxide and graphene quantum dots as electron transport layer," Superlattices and Microstructures, **135**, 106278 (2019). [https://doi.org/10.1016/j.spmi.2019.106278]
[38] K. Weng, L. Ye, L. Zhu, J. Xu, J. Zhou, X. Feng, G. Lu, *et al*., "Molecular design of benzodithiophene-based organic photovoltaic materials to achieve both high VOC and JSC," Nature Communications, **11**, 2855 (2020). https://doi.org/10.1038/s41467-020-16621-x

[39] Y. Zhang, X. Li, T. Dai, D. Xu, J. Xi, and X. Chen, "Charge transport and extraction of PTB7:PC71BM organic solar cells: effect of film thickness and thermal-annealing," RSC Advances, **9**(31), 17857-17864 (2019). https://doi.org/10.1039/c9ra02877c
[40] A. Gusain, R.M. Faria, and P.B. Miranda, "Controlling the morphology and performance of bulk heterojunctions in solar cells: Lessons from interfacial forces," Frontiers in Chemistry, **7**, 61 (2019). https://doi.org/10.3389/fchem.2019.00061
[41] M. Zhang, X. Xu, L. Yu, and Q. Peng, "High-performance ternary organic solar cells with controllable morphology via sequential layer-by-layer deposition," Journal of Power Sources, **506**, 229961 (2021). https://doi.org/10.1016/j.jpowsour.2021.229961
[42] D. Spoltore, W.D. Oosterbaan, S. Khelifi, J.N. Clifford, A. Viterisi, E. Palomares, M. Burgelman, *et al*., "A combined experimental and modeling study of the factors limiting the performance of polymer:fullerene solar cells processed from chlorobenzene and 1,2- dichlorobenzene," Advanced Energy Materials, **3**(2), 227-236 (2013). https://doi.org/10.1002/aenm.201200674
[43] M.R. Khan, and B. Jarząbek, "Recent Advances in Polymer-Based Materials for High-Performance Perovskite Solar Cells," Polymers, **15**(18), 3674 (2023). https://doi.org/10.3390/polym15183674
[44] C. Deibel, Photocurrent in organic solar cells – Part 1, Blog post, Notes on Disordered Matter (2009). https://blog.disorderedmatter.eu/2009/07/20/photocurrent-in-organic-solar-cells-part-1
[45] B. Qi, and J. Wang, "Fill factor in organic solar cells," Journal of Materials Chemistry, **22**(46), 24315- 24325 (2012). https://doi.org/10.1039/c2jm33719c
[46] M. Wright, and A. Uddin, "Organic–inorganic hybrid perovskites: A solution for cost-effective solar cells," Solar Energy Materials, and Solar Cells, **107**, 87–117 (2012). https://doi.org/10.1016/j.solmat.2012.07.006
[47] S. Galindo, M. Ahmadpour, L.G. Gerling, A. Marsal, C. Voz, R. Alcubilla, and J. Puigdollers, "Analysis of the origin of open circuit voltage in organic solar cells with different device architectures," Organic Electronics, **15**(11), 3034-3041 (2014). https://doi.org/10.1016/j.orgel.2014.07.011
[48] Z. Liu, and Y. Lin, "Recent advances in polymer-based interfacial materials for efficient and stable organic solar cells," Polymer Testing, **131**, 108387 (2024). https://doi.org/10.1016/j.polymertesting.2024.108387
[49] A. Kumar, and S. Sharma, "Performance analysis of organic solar cells with different anode buffer layers," IOSR Journal of Electrical and Electronics Engineering (IOSR-JEEE), **14**(4), 49-54 (2019). https://www.iosrjournals.org/iosr-jeee/Papers/Vol14%20Issue%204/Series-1/G1404014954.pdf
[50] J. Yang, X. Wang, X. Yu, J. Liu, Z. Zhang, J. Zhong, and J. Yu, "Recent advances in organic solar cells with non-fullerene acceptors: From morphology control to device optimization," Nanomaterials, **13**(21), 2899 (2023). https://doi.org/10.3390/nano13212899
[51] S. Valsalakumar, S. Bhandari, A. Roy, T.K. Mallick, J. Hinshelwood, and S. Sundaram, "Machine learning-based optimization of hole transport layer-free carbon-based perovskite solar cells," Npj Computational Materials, **10**(1), 94 (2024). https://doi.org/10.1038/s41524-024-01383-7
[52] T.M. Mukametkali, B.R. Ilyassov, A.K. Aimukhanov, T.M. Serikov, A.S. Baltabekov, L.S. Aldasheva, and A.K. Zeinidenov, "Optical and electronic properties of monolayer MoS_2 under different strains: DFT study," Physica B: Condensed Matter, **660**, 414784 (2023). https://doi.org/10.1016/j.physb.2023.414784
[53] S. Sakib, M.Y. Mohd Noor, M.R. Salim, A.S. Abdullah, A.I. Azmi, M.H. Ibrahim and M.H. Ibrahim, "Effect of different composition ratio on structural and morphological properties of TiO_2 nanoparticles synthesized by sol-gel method," Mater. Today: Proc. **76**, 176–182 (2023). https://doi.org/10.1016/j.matpr.2022.11.4564
[54] C. Poelking, J. Benduhn, D. Spoltore, M. Schwarze, S. Roland, F. Piersimoni, D. Neher, *et al*., "Interfacial electrostatics control open-circuit voltage in organic solar cells," Communications Physics, **5**(1), 332 (2022). https://doi.org/10.1038/s42005-022-01084-x
[55] M.R. Khan, and B. Jarząbek, "The effect of 3D printing process parameters on the mechanical properties of PLA polymer and polymer composites: A review," Polymers, **15**(18), 3674 (2023). https://doi.org/10.3390/polym15183674
[56] S.A. Moiz, M.S. Alzahrani, and A.N.M. Alahmadi, "Influence of process parameters on mechanical properties of natural fiber-reinforced polymer composites: A review," Polymers, **14**(17), 3610 (2022). https://doi.org/10.3390/polym14173610
[57] D. Bartesaghi, I. del C. Pérez, J. Kniepert, S. Roland, M. Turbiez, D. Neher, and L.J.A. Koster, "Competition between charge extraction and recombination determines the fill factor in organic solar cells," Nature Communications, **6**, 7083 (2015). https://doi.org/10.1038/ncomms8083
[58] J.C. Nolasco, R. Cabré, J. Ferré-Borrull, L.F. Marsal, M. Estrada, and J. Pallarès, "Design of two-dimensional silicon photonic crystals by means of a guided-mode resonant filter structure," Journal of Applied Physics, **107**(2), 023108 (2010). https://doi.org/10.1063/1.3296294

ВПЛИВ ДОДАТКОВОГО ШАРУ P3HT НА ПРОДУКТИВНІСТЬ ПОЛІМЕРНОГО СОНЯЧНОГО ЕЛЕМЕНТА P3HT: $IC_{60}BA$

Чіттур Девараджан Рамабадран[a,b], К. Себастьян Судхір[a]

[a]*Кафедра фізики, дослідницька лабораторія моделювання оптоелектронних пристроїв, Коледж Христа [Автономний], Іріндžалакуда, Тріссур, 680125, Університет Калікута, Керала, Індія*

[b]*Кафедра фізики, Урядовий коледж, Чіттур, Палаккад, 678104, Університет Калікута, Керала, Індія*

Було проведено моделювання з використанням програмного забезпечення SCAPS 1-D для вивчення впливу додаткового шару P3HT (полі-3-гексилтіофен) на продуктивність сонячних елементів з об'ємним гетеропереходом, зокрема з активним шаром P3HT: IC60BA. Досліджувана структура елемента - ITO/PEDOT:PSS/P3HT/P3HT:IC60BA/ZnO NPs/Al. Після стандартизації програмного забезпечення ми визначили оптимальні параметри структури сонячного елемента, проаналізувавши різні фактори, що впливають на продуктивність елемента в різних шарах. Згодом, після оптимізації структури, ефективність перетворення енергії (PCE) значно покращилася, збільшившись з 5,18% без додаткового шару до 15,26% з додатковим шаром.

Ключові слова: *сонячний елемент з об'ємного гетероперехідного полімеру; фулерен; SCAPS 1-D; активний шар; ETL; HTL*